Influence of the Solar Cycle on the North Atlantic Oscillation

Yuhji Kuroda[1,2], Kunihiko Kodera[1], Kohei Yoshida[1], Seiji Yukimoto[1], and Lesley Gray[3]

[1]Meteorological Research Institute, Tsukuba, Japan
[2]Meteorological College, Kashiwa, Japan
[3]University of Oxford, Oxford, UK

Corresponding author: Yuhji Kuroda (kuroda@mri-jma.go.jp)

Key Points:

1. Propagation of the solar signal can be explained by a top-down mechanism strongly affected by ocean dynamics
2. Solar-related NAO signal tends to peak in February of solar maximum years but shows a 50-year scale drift with lagged amplitudes of ~2 years
3. A positive NAO signal tended to appear earlier in winter as the years since peak solar activity increased

Abstract

We examine the influence of the solar cycle on the North Atlantic Oscillation (NAO) on its pathway from the upper stratosphere to the surface by applying lagged regression analyses to recent observations, historical observations covering 194 years, and an Earth system model simulation covering 165 years. The propagation of the solar signal can well be explained by a top-down mechanism, but one that was strongly affected by ocean dynamics. The solar signal first appears in the subtropical upper stratosphere as a temperature signal. The associated zonal wind signal then propagates downward to the surface in response to stratospheric variability known as the Polar-night Jet Oscillation. The NAO signal tends to appear in February during years of peak solar activity. The solar signal is further modulated such that positive NAO signals tend to appear earlier in winter with increasing years after peak solar activity, which we think to be an oceanic effect. The fluctuations and amplitude modulation of the solar–NAO relationship on a 50-year time scale also suggest that there will be nonlinear interactions between solar forcing and ocean dynamics.

1. Introduction

Radiative energy from the Sun is the most basic of the sources that drive weather and climate. The discovery of sunspots and their temporal variations led to the belief that solar variation could be an important driving force for weather and climate change. Many observational and simulation studies have investigated the influence of solar variability on weather and climate (e.g., Gray et al., 2010). Examples of recent solar–climate research include studies on upper stratospheric ozone (Dhomse et al., 2016), climate change for a future grand solar minimum (Chiodo et al., 2016; Spiegl & Langematz, 2020), historical changes of the North Atlantic winter climate (Ma et al., 2018), and changes of the Walker circulation (Misios et al., 2019).

Satellite observations of the 11-year solar cycle have shown only very small changes (~0.1%) in solar irradiance (Kopp & Lean, 2011), but large changes of 4–8% in the 200–250 nm wavelength range of the ultraviolet (UV) spectrum (Lean et al., 1997). Therefore, there is a well-documented 11-year cycle of the solar-induced temperature signal associated with variations in UV absorption and changes of ozone levels in the stratosphere (Gray et al., 2010). These temperature changes affect the background winds that influence the propagation of planetary waves through their relationship with thermal winds (Kodera & Kuroda, 2002). As a result, the internal mode of variability in the polar night jet is modulated such that the early winter solar signal in the subtropical stratopause triggers the downward propagation of anomalous zonal wind, and an anomalous annular pattern in the sea level pressure (SLP) tends to appear in mid-winter (Kodera, 1995; Kodera & Kuroda, 2002; Kuroda & Kodera, 2002). In the North Atlantic region, it is represented by the modulation of an important mode of climate variability known as the North Atlantic Oscillation (NAO). The climate in North America, Europe, and Eurasia is strongly influenced by the NAO (Hurrell et al., 2003). This process has been well reproduced by simulations with a chemistry–climate model (Matthes et al., 2004, 2006; Mitchell et al., 2015). Thus this “top-down mechanism” plays a crucial role in conveying solar signals to the surface.

Recently, however, the role of the ocean in solar–climate interactions has begun to attract attention (e.g., Misios et al., 2019). If this “bottom-up mechanism” (Meehl et al., 2009) is applied to the North Atlantic, the solar signal will be received by the ocean through forcings of the solar-related NAO, but the NAO will also be forced by Sea Surface Temperature (SST), which is controlled by ocean dynamics. Thus, the NAO will be created through the interaction of both of these dynamics. The results of recent numerical experiments conducted with the UK Met Office model have shown that in the

North Atlantic region the response of the NAO signal to the oceanic signal is delayed relative to the solar cycle because of the ocean's large thermal inertia (Andrews et al., 2015; Ineson et al., 2011; Scaife et al., 2013), which is consistent with recent analyses using historical observational data (Gray et al., 2013, 2016).

However, Chiodo et al. (2019) concluded that NAO-related solar signals since the mid-1960s might have been a chance occurrence due to internal variability and suggested that the model simulations of past solar–climate studies (e.g., Thiéblemont et al., 2015) are either statistically insignificant or absent. This conclusion has important implications for understanding the solar–NAO relationship and needs to be explained in detail. For this reason, we re-examined the relationship by using comprehensive observational data and undertook realistic long-term simulations.

This paper is organized as follows. Section 2 describes the data and analytical methods, Section 3 presents the results, which discussed in Section 4.

2. Data and Analysis Methods

For recent observational data, we used mainly ERA-Interim reanalysis data from the European Centre for Medium-range Weather Forecasts (Dee et al., 2011) for the period January 1979 to June 2017. Because the reanalysis did not take account of the influence of solar activity, the data tend to be inaccurate in the upper stratosphere in particular, where both the radiative influence of UV radiation and the chemical influence of nitric oxide, which is produced in the mesosphere by incoming solar protons and strongly influences ozone levels (e.g., Bailey et al., 2002), have large impacts. Therefore, we used zonal-mean satellite observation data for atmospheric levels higher than 5 hPa (~37km). Specifically, for our analyses we used satellite data from the US National Centers for Environmental Prediction/Climate Prediction Center (NCEP/CPC, formerly NMC/CAC) for the period January 1979 to June 2007, and November 2008 to June 2017. No satellite data of NCEP/CPC were available for the relatively long period between June 2007 and November 2008; this gap was filled by using bias-corrected Aura-MLS satellite analysis data from the US National Aeronautics and Space Administration (Schwartz et al., 2008). Note that the Aura-MLS reanalysis data were used only to complement the NCEP/CPC satellite data. The satellite data include temperature and geopotential height data, and we calculated zonal wind from the latter by assuming a balanced wind relationship north of 15°N. We calculated monthly zonal-mean values from the daily values provided in the satellite datasets and used only zonal-mean monthly values for the analysis. We made no adjustments to account for the boundary between the satellite data and the ERA-Interim data. We also

used the Eliassen–Palm flux (E-P flux) and residual velocities calculated from the ERA-Interim daily data up to 1 hPa to examine the role of dynamical effects on the solar-NAO coupling. For definitions of the E-P flux and residual velocities see, for example, Andrews et al. (1987).

Although we consider the above observational data to be accurate and comprehensive, the length of the data record is only about 38 years. Therefore, we also conducted analyses using two reliable historical observational datasets that cover 194 years (from 1823 to 2016): a historical station-based NAO index (Jones et al., 1997), and a solar activity dataset based on sunspot numbers. The NAO index was provided by the University of East Anglia Climate Research Unit, UK, and the Sunspot Number (SSN) data were provided by the Royal Observatory of Belgium. To examine SST, we used monthly Extended Reconstructed Sea Surface Temperature version 5 (ERSSTv5) data (Huang et al., 2017) provided by the National Oceanic and Atmospheric Administration (NOAA) for 1854 to 2017. To remove the trend component of the original data, we removed 55-year running averages to provide our basic SST dataset.

In addition to the recent and historical observational datasets, we used data from a long-term historical simulation obtained by using the Earth system Model Ver. 2 of the Meteorological Research Institute (MRI) of Japan (Yukimoto et al., 2019). This model has four components: atmosphere, ocean, aerosol, and atmospheric chemistry. The atmosphere model has 80 levels in the vertical with the top level at 0.01 hPa, and its horizontal resolution is TL159 (~120 km). The radiation scheme is the same as that in the MRI-CGCM3 model (Yukimoto et al., 2012), and the radiative flux is calculated in 9 long-wave bands and 22 short-wave bands that include the visible and UV regions. The simulation was carried out for the period from 1850 to 2014 using the Coupled Model Intercomparison Project Phase 6 (CMIP6) configuration, which takes account of changes in spectral solar irradiance and high-energy particle precipitation (Matthes et al., 2017), historical Earth orbital change, variations in volcanic and other aerosols, and historical changes in greenhouse gas concentrations and land use (see Eyring et al. (2016) for more details). The atmospheric chemistry component calculates ozone concentrations interactively. The Earth system Model can reproduce the equatorial Quasi-Biennial Oscillation (QBO) with a realistic period of about 28 months by using the non-orographic gravity wave parameterization scheme of Hines (1997). After setting atmospheric, well-balanced oceanic, and other initial conditions as described in Yukimoto et al. (2019), a pre-simulation spin-up of 40-years was conducted to allow the oceanic state to reach equilibrium.

We performed lagged regression analyses on the recent observations, historical

observations, and the long-term simulated historical dataset against proxies for solar activity. For example, the lagged regression of the i-th spatial grid of SST for the lag of the k-th year is calculated by

$$R(x_i,k)=\left\langle Z(x_i,t_j)\hat{S}(t_{j-k})\right\rangle_j, \quad (1)$$

where $Z(x_i,t_j)$ is the SST at the i-th spatial grid of the j-th year, $\hat{S}(t_{j-k})$ is the standardized proxy of a solar activity at the $j-k$-th years, and $\langle\ \rangle_j$ means averaging over all the years of j. The statistical significance is evaluated based on the lagged correlation (Maisel, 1971) defined by

$$C(x_i,k)=\left\langle \hat{Z}(x_i,t_j)\hat{S}(t_{j-k})\right\rangle_j, \quad (2)$$

where $\hat{Z}(x_i,t_j)$ is the standardized SST satisfying $\left\langle \hat{Z}(x_i,t_j)^2\right\rangle_j=1$ for all x_i.

As proxies for solar activity, for the recent observations, we used the annual mean solar radio flux at 10.7 cm in "solar flux unit" of 10^{-22} Wm^{-2} Hz^{-1} (F10.7 index). For the historical observations, we used annual mean SSN (dimensionless), and for the simulated historical data we used the decadal component of total solar irradiance (TSI, Wm^{-2}). We used different 11-year solar indices for the various datasets because the F10.7 index can be obtained only from 1947, but it is well-correlated with SSN measured since 1749. Similarly, because satellite observations show the 11-year component of TSI to be well correlated with both the F10.7 index and SSN (Gray et al., 2010), we used the decadal component of TSI for analysis of the simulation.

We obtained the decadal component of TSI by first removing 55-year running averages from the original data to remove prominent 100-year scale trends and variations, and then calculating annual averages. Note that the 100-year scale trends and variations exist only for TSI and not for indices used for the observational data. Before our analyses, we applied the same filtering procedure to all simulated data to remove low-frequency variability such as the effect of global warming.

For the recent observations and model simulation, the NAO was defined as the leading month-to-month variability of SLP during extended winter (November to April) for the North Atlantic region from 20° to 70° N and from 90° W to 40° E, following the definition of Hurrell et al. (2003). The observational data show that the NAO explains 34% of the total variance, far more than the second mode, which explains only 20%. The spatial pattern we obtained was a typical meridional dipole with its negative center

(–7 hPa) over Iceland and its positive center (4 hPa) over the Azores (not shown). The modeled NAO was very similar to that of the observational data except that the positive center over the Azores was 5 hPa (not shown).

Because our attention is focused on the variations of the boreal winter associated with the 11-year solar cycle, we used annual mean indices by averaging monthly indices from July of one year to June of the next year. We carried out both simultaneous regression analyses and lagged analyses. For the lagged analyses, we calculated the positive lag by using time-shifted solar index data with the same data length as the data for the simultaneous analyses. To calculate the negative lag, we shortened the data length as necessary because future values of the F10.7 and SSN indices were not available. For the simulated data, however, CMIP6 recommended future TSI data were used without shortening.

3. Results

3.1. Recent Observations

In our analyses of recent observational data, we used the observed annual mean F10.7 index data for 1973–2016 (Figure 1). Here, we identify each winter according to the year in which the December of that winter fell (i.e., winter of 2000 means the winter of 2000–2001). The period 1973–2016 includes almost four complete 11-year solar cycles.

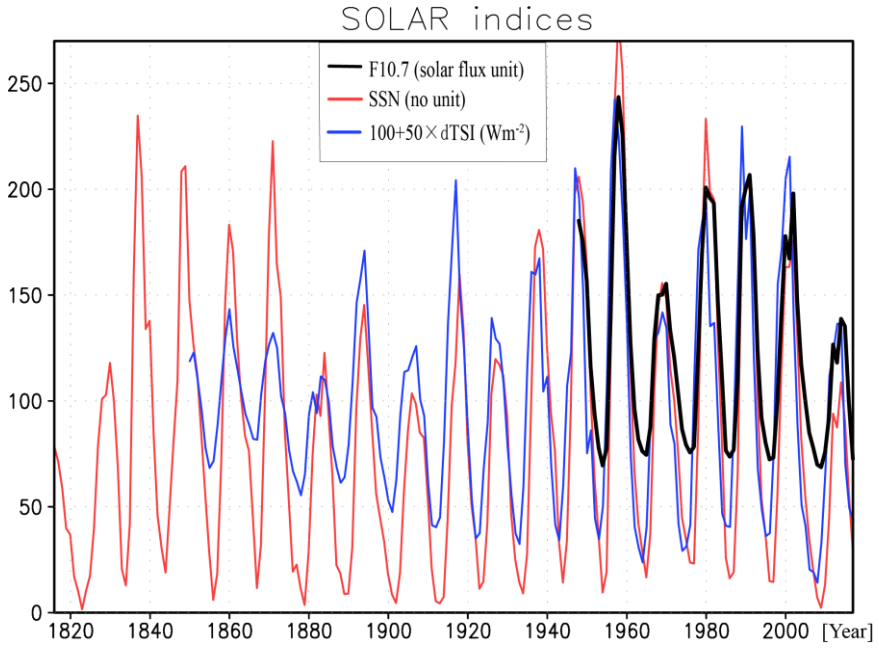

Figure 1. Time series of various annual mean solar indices from 1815 to 2016.

The regression results for zonal-mean temperature during the northern winter

(November–March) against the annual mean F10.7 index with zero lag shows that

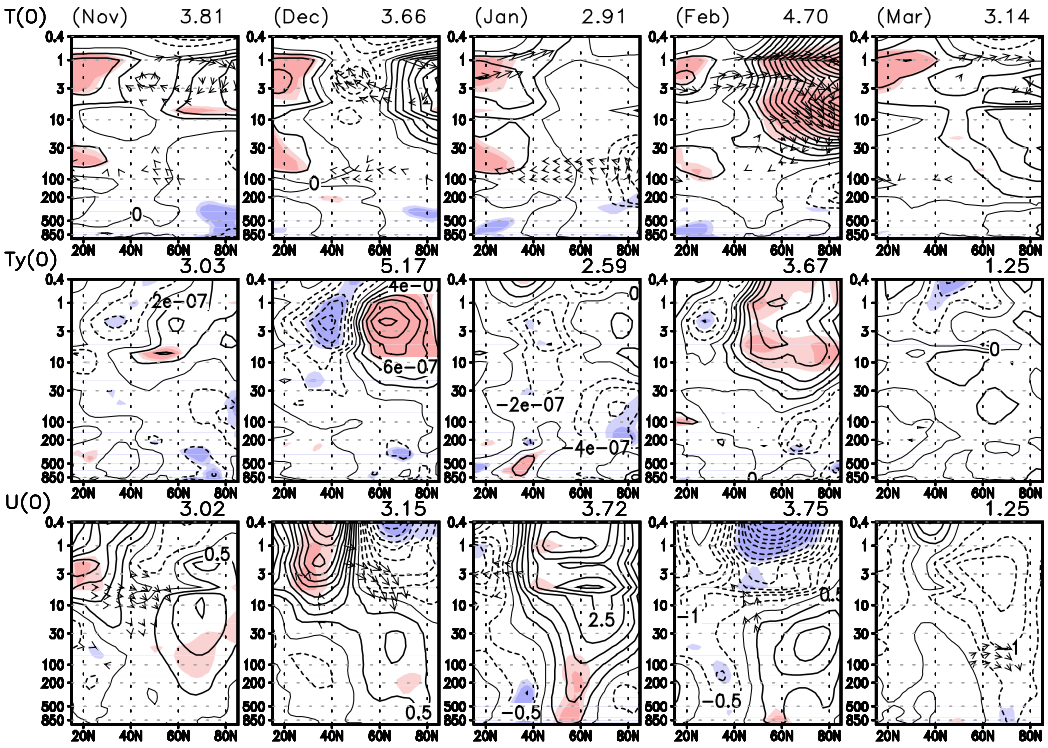

Figure 2. Regressions of observed (upper row) zonal-mean temperature and residual velocities, (middle row) zonal-mean meridional temperature gradient, and (bottom row) zonal-mean zonal wind and E-P flux against annual mean F10.7 index from November to March in lag-0 year from 1979 to 2017. The *y*-axis indicates height (hPa). The *x*-axis indicates latitude (15°N to 85°N). Light (dark) shading (red positive, blue negative) indicates areas of greater than 90% (95%) statistical significance. Only regressions of residual velocities and E-P flux with larger than 95% statistical significance are shown. Contour intervals are 0.3 K for temperature, 2×10^{-7} K m^{-1} for the meridional temperature gradient, and 0.5 m s^{-1} for zonal wind. E-P flux has been scaled by the reciprocal square root of pressure. Dashed lines indicate negative values. Numbers annotated above (upper right) each panel indicate percentage of variance explained by the solar cycle, calculated by areal averaging of squared correlations.

from November to December, regions of higher temperature around the stratopause tended to appear at latitudes lower than 30°N (Figure 2, upper row). This distribution can be explained by increased UV radiation according to the climatological latitudinal distribution of the solar flux during years of high solar activity because UV radiation directly heats the stratosphere by means of an ozone feedback process (Kodera & Kuroda, 2002; Kuroda & Kodera, 2002). In addition, a temperature minimum in the stratopause near 50°N and polar heating in the upper stratosphere from November to December were

produced by a dynamically driven meridional circulation associated with reduced upward propagation of the E-P flux corresponding to enhanced zonal wind in the upper stratosphere at low latitudes.

The zonal-mean temperature profile showed a large negative meridional temperature gradient at around 40°N at the 2 hPa level from November to December (Figure 2, middle panels), although the gradient in November was not statistically significant. There was a positive signal at around 60°N; thus, a meridional dipole structure appeared there from November to December, with the December dipole more significant. Zonal-mean zonal wind signals, which are associated with the meridional temperature gradient in the upper stratosphere (Figure 2, lower panels), can be explained by the thermal wind relationship. In particular, a significant positive wind signal at around 20°N at 1 hPa in November was amplified and shifted to around 30°N and 0.4 hPa in December, although it was less significant in December. This positive anomalous wind signal then shifted poleward and downward in subsequent months until February when it was in the lower polar stratosphere. This poleward and downward movement of the anomalous zonal-mean zonal wind represents natural variability caused by the interaction of planetary waves with the zonal-mean field in the winter stratosphere, which is known as the Polar-night Jet Oscillation (PJO) (Kuroda & Kodera, 2001) and is not directly related to solar activity. However, PJO activity causes the solar signal created in the upper subtropical stratosphere in early winter to move downward during subsequent months. We have proposed this top-down mechanism of solar influence in our previous studies (Kodera & Kuroda, 2002; Kuroda & Kodera, 2002).

We next examined the effect of the solar cycle on the SLP in the North Atlantic (Figure 3). We found that a meridional dipole structure characterized by anomalously low (high) SLP tended to build in the northern (southern) part of the North Atlantic from January to February for lags of –1, 0, and +1 years. This pattern is comparable to the pattern associated with the positive phase of the NAO.

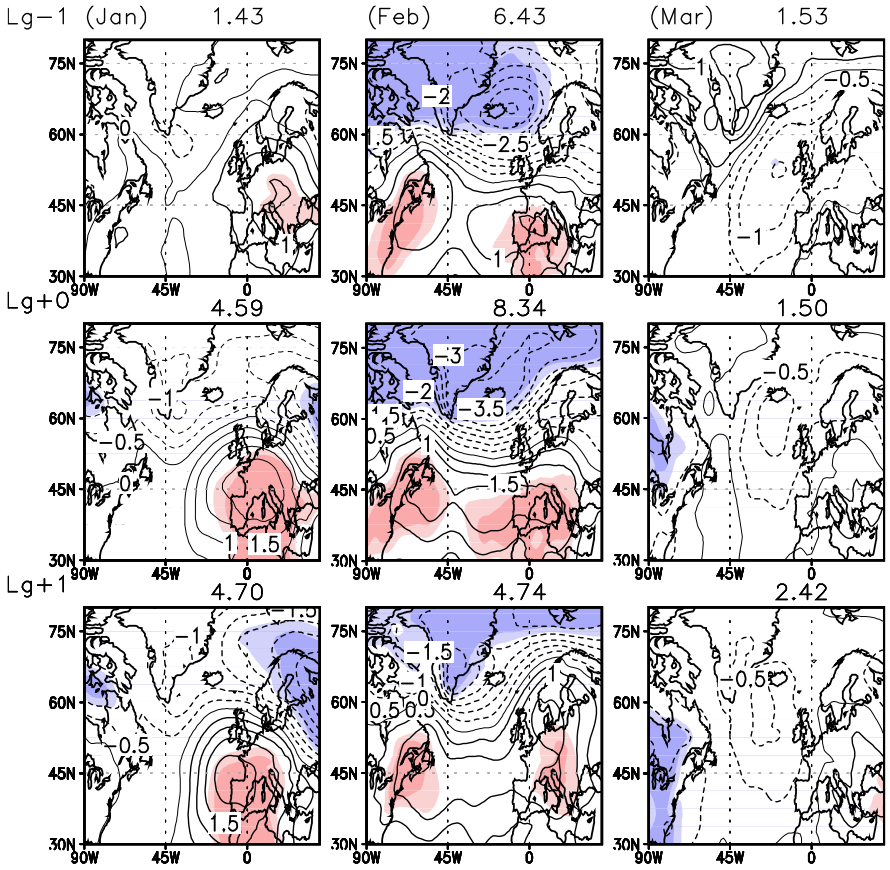

Figure 3. Lagged regressions of observed SLP (contour interval 0.5 hPa, negative values shown as dashed lines) against annual mean F10.7 index from January to March (columns) for lag years –1, 0, and +1 (top to bottom) from 1980 to 2017. Dark (light) shading (red, positive values; blue, negative values) indicates areas of greater than 95% (90%) statistical significance. The positive lags correspond to the years when solar activity leads SLP. Numbers annotated above (upper right) each panel indicate the percentage of variance explained by the solar index, calculated by areal averaging of squared correlations.

To examine the evolution of the PJO during the seasonal march, it is convenient to use PJO space (Kuroda & Kodera, 2004), which is defined by the first two principal components (PC1 and PC2) of the empirical orthogonal functions (EOFs) of anomalous polar temperatures (see Appendix A). Thus, the stratospheric state in the i-th month and the j-th year can be represented by the two-dimensional PJO space $\left(P_1(m_i,t_j), P_2(m_i,t_j)\right)$, where $P_1(m_i,t_j)$ and $P_2(m_i,t_j)$ are PC1 and PC2 for the i-th month of the j-th year, respectively. The lagged regression of PC1 against annual mean F10.7 index for the i-th month of lag of k-th year can be calculated by

$$\mathrm{P1}(i,k) = \left\langle P_1(m_i,t_j)\hat{S}(t_{j-k})\right\rangle_j , \qquad (3)$$

where $\hat{S}(t_{j-k})$ is the standardized F10.7 index for the $j-k$ -th years, and $\langle\ \rangle_j$ means averaging over all the years of j. From these regressions $(\mathrm{P1}(i,k),\mathrm{P2}(i,k))$, regressed amplitude $A(i,k)$, and phase angle $\theta(i,k)$ are calculated as

$$A=\sqrt{\mathrm{P1}^2+\mathrm{P2}^2},\qquad \theta=\tan^{-1}\frac{\mathrm{P2}}{\mathrm{P1}}. \tag{4}$$

Thus, the amplitude $A(i,k)$ is the distance of the regressed state vector from the origin and the phase angle $\theta(i,k)$ is measured counterclockwise from the positive part of the x axis (PC1). The statistical significance of PC1 and PC2 can be evaluated from the correlation with the annual mean F10.7 index. From them the statistical significance of the amplitude is simply calculated as Eq. (4). Note that phase angles are calculated to be between –180° and +180°. Thus, special attention is needed when there are state vectors on or near the negative PC1 axis, because they appear as tightly packed contours on either side of the zero contour (e.g., January at a lag of –4 years in Figure 4a). However, because we focused mainly on the area around the zero phase angle (i.e., the positive region on the x axis) which is closely related to the positive NAO during periods of high solar activity, this was not problematic.

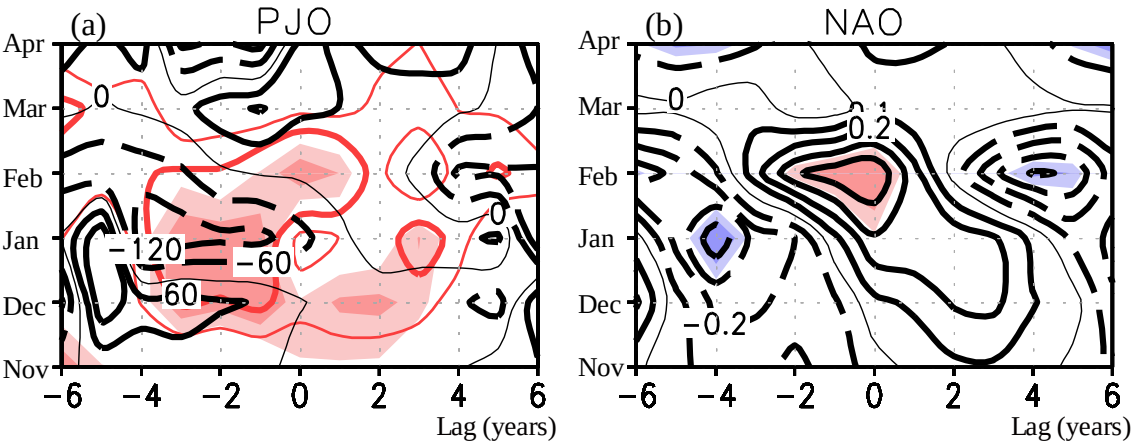

Figure 4. Lagged regressions of observed (a) PJO indices and (b) NAO index against annual mean F10.7 index from 1979 to 2017. PJO indices are represented by their amplitudes (red contours) and phase angles (degrees, black contours). Thick (thin) red contours indicate values of 0.3 (0.2). Dark (light) shading (red, positive, blue negative) indicates areas of greater than 95% (90%) statistical significance. Black contours in (a) are at 60° intervals; those in (b) are at 0.1 intervals, and negative values are shown by dashed lines in both (a) and (b). Thin black line shows zero. Positive lags represent years when solar activity leads the PJO or the NAO indices.

The amplitude of the PJO tended to be large from December to February for lags of –3 to 0 years. During this period, the state vector rotated counterclockwise with the seasonal march. For example, at the 0-year lag, the phase angle increased from –60° to +60° from January to March.

Kuroda and Kodera (2004) have shown that, in association with the time evolution of the PJO, the positive (negative) phase of the Arctic Oscillation, and thus that of the NAO, tends to appear on the positive (negative) *x*-axis (PC1). Thus, the positive phase of the NAO appears at around zero phase angle in PJO space.

The lagged regression of the NAO index against the annual mean F10.7 index (Figure 4b) was consistent with that of the PJO against the solar index (Figure 4a) in that it showed significantly large positive NAO index values (peak value 0.4) around February for the 0-year lag. Note that the standard deviation of the NAO index in February is 1.2, at which time the peak value is rather large. In addition, the peak of the NAO index tended to appear earlier in winter as the lag in years increased, consistent with the zero phase angle configuration of the PJO (Figure 4a).

To highlight the effect of the pathway of the solar cycle on the NAO more clearly, we considered the time evolution of key quantities as functions of both the lag of years and the months of winter (Figure 5). In association with the 11-year solar cycle, both the December–January–February (DJF)-mean equatorial temperature and the December-mean subtropical meridional temperature gradient at the stratopause tended to peak at the 0-year lag. For the same year, the state vector in PJO space tended to intersect the positive PC1 axis from January to February. The amplitudes of the February-mean PJO index and the February-mean NAO index also tended to peak at the 0-year lag (Figure 5a). The close relationship between the PJO and NAO was also evident in their seasonal evolutions at their 0-year lags. In fact, with the seasonal evolution from January to February, the phase of the PJO increased, and the amplitudes of the PJO and NAO tended to peak in February when the phase of the PJO approached zero (Figure 5b).

Our results thus suggest that these variables vary as a set with the change of the 11-year solar cycle, which is therefore consistent with the previously proposed top-down mechanism (Kodera & Kuroda, 2002; Kuroda & Kodera, 2002).

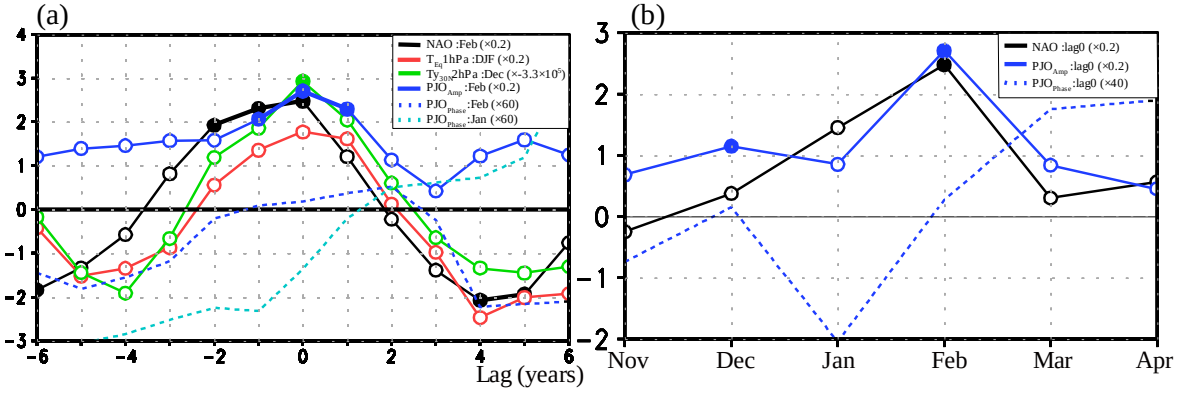

Figure 5. (a) Lagged regressions of various observed atmospheric quantities against annual mean F10.7 index from 1979 to 2017. Positive lags correspond to years when solar activity leads the other indices. (b) Winter evolution of the NAO-index and PJO-indices regressed against the annual mean F10.7 index at 0-year lag. The values of each atmospheric quantity at each point on its curve can be calculated by multiplying the corresponding value on the *y*-axis by the number in parentheses in the legend description. The units of measure for equatorial temperature at 1 hPa ($T_{eq}1hPa$), meridional gradient of temperature at 30°N and 2 hPa ($Ty_{30N}2hPa$), and phase of the PJO index (PJO_{phase}) are K, K m^{-1}, and degrees, respectively. On each curve, thick lines and closed circles indicate statistical significance higher than 90%.

3.2. Historical Observations

Although there are few parameters for which long-term observational data are available, those that are available can provide very reliable data, in particular, historical station-based NAO index values and solar activity based on SSN. We therefore performed lagged regression analyses of the long-term observational NAO index data, similar to the analyses described above for the recent observational data.

The historical station-based NAO index was highly correlated with the EOF-based NAO index described in section 3.1 for the 38 overlapping years (1979–2016); the correlation coefficient (r) of the relationship for the 38 winters (November to April) was 0.88, and that for the 38 DJF means was 0.97. Similarly, the historical SSN-based annual-mean solar activity correlated well with the F10.7 index (for 1947–2016, r = 0.99). Therefore, comparisons of those observational results with results based on the historical station-based NAO and SSN data will be meaningful.

The structure of the solar–NAO relationship based on the 194-year data series (Figure 6) was very similar to that of the solar–NAO relationship for the period from 1973 to 2017 (Figure 4b). In both cases, an NAO index peak appeared in February of 0-lag years, and negative peaks appeared in February of lag –5 and +5 years. It is noteworthy that the change to a positive NAO index value tended to appear earlier in winter as the lag increased. However, even though the dataset covered a much longer period, the statistical significance of the signals was not very strong.

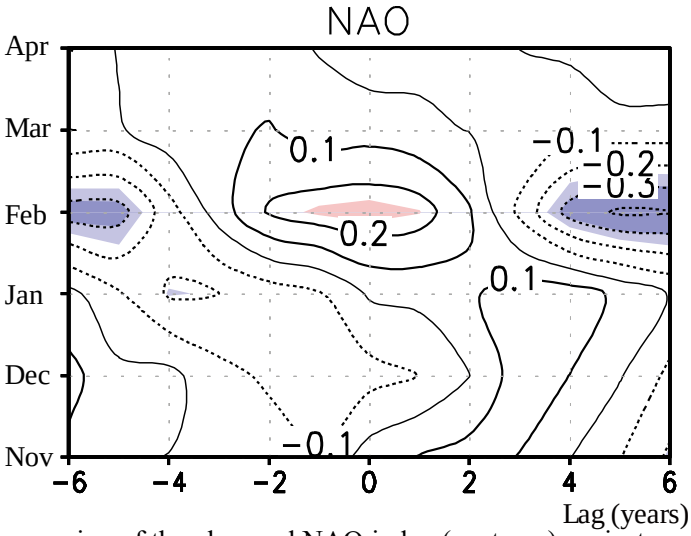

Figure 6. Lagged regression of the observed NAO index (contours) against annual mean SSN using monthly NAO-index data from 1823 to 2017. The contour interval is 0.1 and negative values are shown by dotted lines. Dark (light) shading indicates areas of higher than 95% (90%) statistical significance. Red (blue) shading indicates positive (negative) values.

To investigate the temporal changes of the solar–NAO relationship during 1823–2017, we performed lagged regression analyses for running 41-year mean monthly values of the NAO index for each year using a similar approach to that of Ma et al. (2018). The lag years for peak February-mean NAO (Figure 7a) drifted between about –2 and +2 years, and there were large temporal changes in the amplitude of the peak values. For example, the NAO tended to peak at 0.4 around a lag of –2 years for the period centered at 1860 and at 0.8 around lags of 1–2 years for the period centered at 1970. In contrast, the amplitude of the peak was very low for the period centered at 1930. However, it is noteworthy that positive NAO signals tended to appear only near lag 0 throughout the entire period analyzed, although the peak showed a 50-year scale drift with an amplitude of about 2 years.

To see how the month of peaked NAO changed over a longer time scale, we performed similar 41-year regression analyses without lags (Figure 7b). The positive NAO signal appeared predominantly in February without evidence of a decadal drift to other months. However, a decadal change of the signal strength was evident. The signal strength was relatively strong for periods centered at 1840, 1910, 1950, and 1970 and subsequent years, although the signal was significant only for periods centered on years after 1970. However, significant peaks tended to appear in February for lag +1 to +2 years from 1940 to 1980 and for lag –2 years prior to 1920 (Figure 7c). Thus, the existence of a dominantly positive February NAO signal throughout the period 1823–2017 is noteworthy.

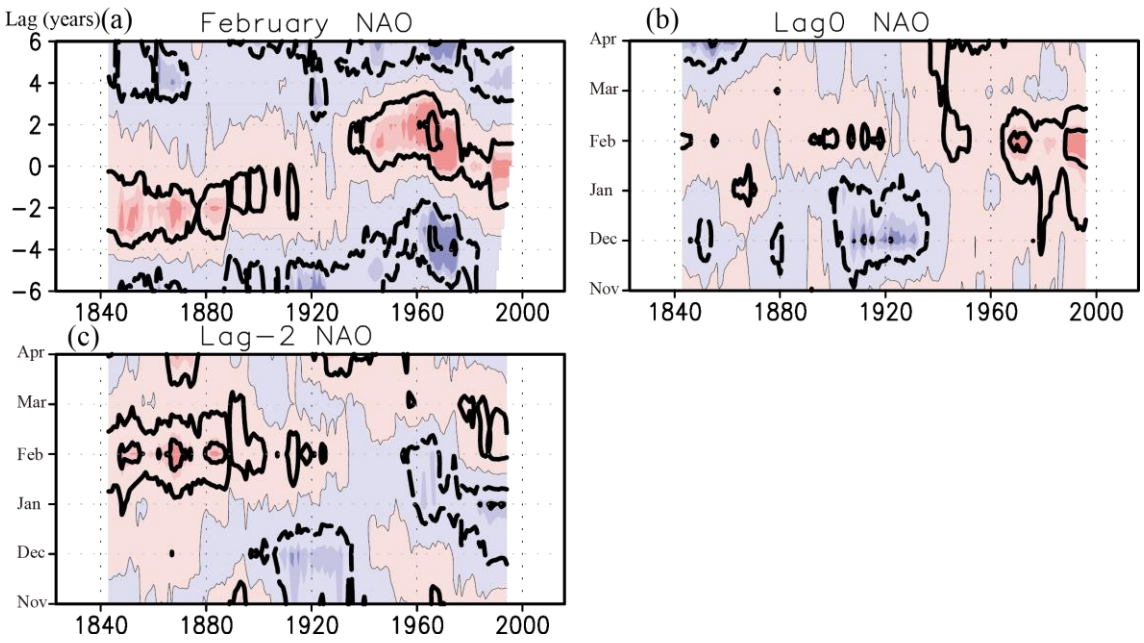

Figure 7. (a) Lagged regression of the observed February-mean NAO index (contours) against annual mean SSN data from 1823 to 2017. The *x*-axis shows the central years for each of the 41-year running calculations at yearly increments. The shading indicates polarity (red positive, blue negative). The darkest (middle) shading indicates higher than 95% (90%) statistical significance. The contour interval is 0.4 and the thin line is the zero contour. (b) Same as (a) but for the lag 0 regression of the NAO index for each winter month. The contour interval is 0.3 and the thin line is the zero contour. (c) Same as (b) but for the lag –2 years regression.

It is well known that the NAO is closely related to the variability of the SST (Hurrell et al., 2003). Thus, we examined how the SST is influenced by the solar cycle and how they are both related to the NAO by using the detrended 163-year historical record of the ERSSTv5 data. Our regression maps for winter (November to April; Figure 8a to 8c) mean SSTs for lags of 0, 2, and 4 years are similar to those of Kodera et al. (2016; their Figure 9). At the solar peak year (lag 0), small, positive SST anomalies (SSTAs) appear only near the east coast of the United States (US) and along the west coast of Africa. For a lag of 2 years, the positive SSTA near the east coast of the US extends to the northeast across the Atlantic and reaches a peak of 0.08 K at around 35°N and 50°W. For a lag of 4 years, the positive SSTA extends farther to the northeast with its peak reaching 0.09 K at around 45°N and 45°W. Although the shape and amplitude of this SSTA tend to change with the seasonal march, that change is smaller than the interannual change and corresponds better to the longer timescale (~1 year) of the SST.

Such solar-related SST patterns have some similarity with the so called “NAO

SST tripole" pattern, which is obtained by regressing SST against the NAO index (Hurrell et al., 2003). Thus, to simplify our analysis, we have evaluated solar-related NAO changes of the SST by using the index of the NAO SST tripole (called the SST-NAO index). Although both the month-to-month and year-to-year regression patterns show typical tripole patterns, here we used the simpler decadal pattern, which we obtained by regressing low-frequency SST against low-frequency NAO (Figure 8d), both with cutoff frequencies of 8 years. The derived pattern is roughly horseshoe shaped similar to that obtained in the lagged analysis (Hurrell et al., 2003). The monthly SST-NAO index is then defined by projecting the anomalous SST onto the basic pattern for the area from 10°N to 60°N and 80°W to 0°E with standardization.

The lagged regression of the SST-NAO index for each month of winter against the annual mean SSN (Figure 8e) shows that the index tends to peak for a lag of 2 years and that the seasonal change is relatively small, although it tends to be stronger in November. The pattern of the lagged regression of the SST-NAO indices for January using running 41-year means of monthly data (Figure 8f) can be regarded as the typical winter pattern because it changes little during the winter months. It is noteworthy that the same calculation for a specific month by treating monthly mean values as annual values gave a similar pattern, probably corresponding to the longer timescale of the SST (not shown). If we compare the solar-related SST-NAO signal with that of the February NAO (green lines in Figure 8f), the former tends to be delayed by 2 to 3 years relative to the latter from 1870 to 1890 and from 1960 to 2000, when solar-synchronous SST signals were more prominent. In fact, the peak of the SST-NAO signal is at lag 3 years, whereas that of the February NAO index is at lag 1 year for 1970. In contrast, the SST-NAO tends to lead by 1 to 2 years from 1940 to 1960, when the NAO amplitude was moderate. However, the SST-NAO was completely out of phase with the February NAO index from 1900 to 1940 when the NAO was weaker. Note that the precedence of the NAO index relative to the SST-NAO index, for example, does not necessarily mean that the NAO alone forces the SST-NAO; rather, their variabilities are mutually sustained for specific lag times, because both indices tend to correlate over a wide range of lag times (Hurrell et al., 2003). Our analysis suggests that there are strong interactions between the solar-related NAO and the SST for relatively long periods, although there are also weaker coupling periods. It is noteworthy that the close relation of solar-related SST to the NAO applies only for the month of February, suggesting that solar-related SST is caused mainly by the top-down mechanism of the NAO.

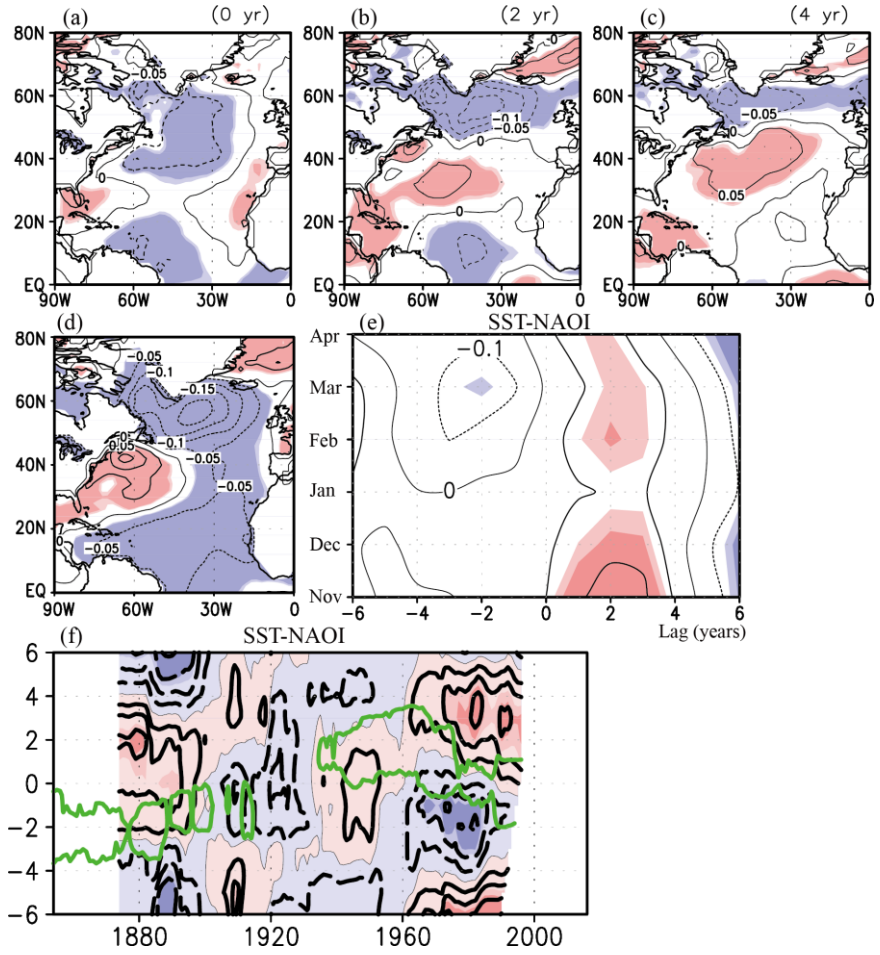

Figure 8. (a)-(c) Lagged regressions (contours) for lags of (a) 0, (b) 2, and (c) 4 years of observed winter-mean SST in the North Atlantic against annual mean SSN from 1854 to 2017. The contour interval is 0.05 K; negative contours are shown as dashed lines. Red and blue shading indicate positive and negative values, respectively. Areas of darker (lighter) shading indicate statistical significance higher than 95% (90%). (d) Same as panel (a), but showing the regression (contours) of the low-frequency component (T > 8 years) of SST against the low-frequency component (T > 8 years) of the NAO. (e) Same as panel (a), but showing the lagged regression of the SST-NAO index (contours) against annual mean SSN using monthly SST-NAO data from 1854 to 2017. The contour interval is 0.1. The *x*-axis shows lag years; a positive lag means SSN leads SST-NAO. (f) Lagged regression of the January low-frequency component of the SST-NAO index (contours) against monthly SSN data from 1854 to 2017. The *x*-axis shows the central years for each of the 41-year running means at yearly increments. The *y*-axis shows the lag years. The contour interval is 0.1. Red and blue shading indicates positive and negative values, respectively. Areas of darker (lighter) shading indicate statistical significance higher than 95% (90%). The green contours show the same regression for the value of 0.4, but using the NAO index for February.

3.3 Simulated 1850–2014 data

We also performed a lagged regression analysis for the period from 1850 to 2014 using data simulated by the MRI Earth system Model. For this analysis we used the standardized decadal component of total solar irradiance (dTSI) as a proxy for solar activity, which is correlated with the other solar indices in the observational data (Gray et al., 2010). Because raw TSI data include a component of a low-frequency, long-term trend, we extracted the decadal component by removing low-frequency variability. Comparison of the scaled dTSI index time series (= 100 + 50 × dTSI; blue line in Figure 1) with other solar indices used in this study showed that the phase of the dTSI index matched the other indices well, although the amplitude of the dTSI index appeared to show an overall gradual increase after the 1850s. For the regression analysis, we used the same time filter that was used to construct the dTSI index to remove the low-frequency, long-term trends from the modeled data.

The lag-0 regression results (Figure 9) showed that a significant temperature signal at the subtropical stratopause tended to appear throughout the winter, as was the case for the observed data. Significantly anomalous westerly winds in the subtropical upper stratosphere in November appeared to be associated with this signal, which subsequently extended downward then moved poleward and created anomalous westerlies around 50°N of the lower troposphere in December and January. Thus, the MRI model produced the downward propagation of the solar signal associated with the PJO well, though it was faster and less prominent than in the observational data (1979-2017).

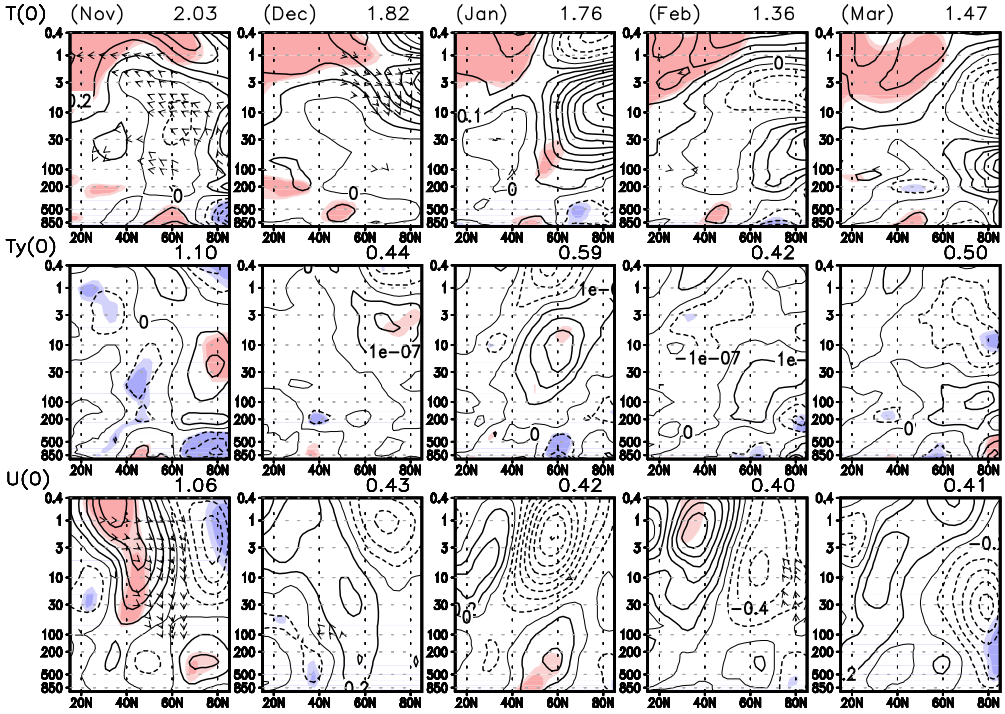

Figure 9. Regressions of simulated (upper panels) zonal-mean temperature and residual velocities, (middle panels) meridional gradient of temperature, and (lower panels) zonal-mean zonal wind and E-P flux against annual mean decadal TSI from November to March for lag 0 year from 1850 to 2014. The *y*-axis indicates height (hPa). The *x*-axis indicates latitude (15°N to 85°N). Light (dark) shading (red positive, blue negative) indicates areas of greater than 90% (95%) statistical significance. Only regressions of residual velocities and E-P flux with larger than 95% statistical significance are shown. Contour intervals are 0.1 K for temperature, 1×10^{-7} K m^{-1} for meridional temperature gradient, and 0.2 m s^{-1} for zonal wind. E-P flux has been scaled by the reciprocal square root of pressure. Dashed lines indicate negative values. Numbers annotated above (upper right) each panel indicate the percentage of values explained by the solar cycle, calculated by areal averaging of squared correlations.

The lagged results for regression of the PJO against the dTSI index (Figure 10a), where the PJO was defined on the basis of anomalous polar temperatures (see Appendix A), showed the modeled EOF1 (EOF2) to be very similar to the EOF2 (EOF1) obtained for the observed data. Therefore, we defined PJO space by using PC2 as the *x*-axis and PC1 as the *y*-axis, with phase angle again measured counterclockwise from the positive region of the *x*-axis. Together, EOF1 and EOF2 explain almost 95% of the variance of anomalous polar temperatures; thus, the use of PJO space in our analysis is justified.

During December to March at lags of around –4 to 0 years, the simulated phase angle structure was somewhat similar to that obtained from the observational data; the phase tended to increase from lower left to upper right (Figure 4a). However, the amplitude tended to be lower, especially in January at a lag of around –1 year.

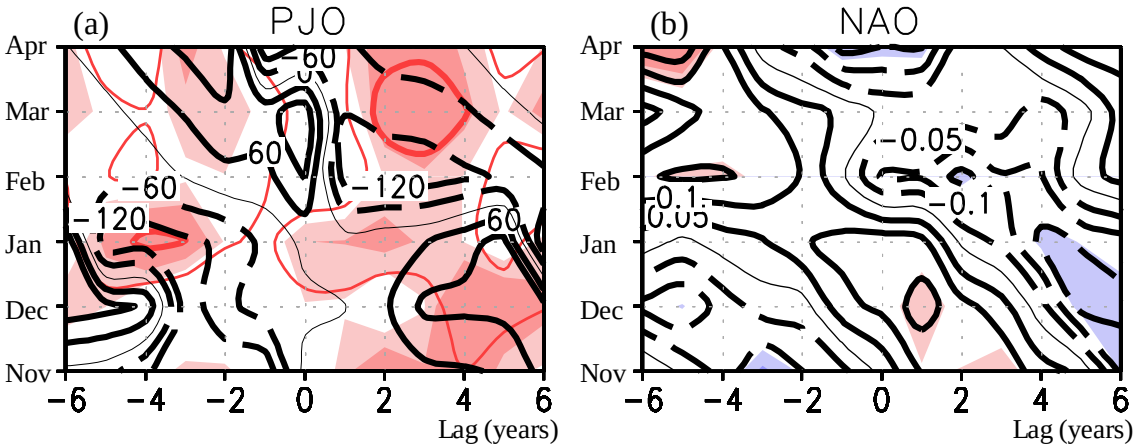

Figure 10. Lagged regressions of simulated (a) PJO indices and (b) the NAO index against annual mean dTSI index from 1850 to 2014. The PJO indices are represented by their amplitude (red contours)

and phase angle (degrees, black contours). Thick (thin) red contours indicate 0.2 (0.1). Dark (light) shading (pink, positive values; blue, negative values) indicates areas of greater than 90% (80%) statistical significance. Black contours in (a) are at 60° intervals; those in (b) are at 0.1 intervals with negative values shown as dashed contours. Positive lags represent years when solar activity leads.

Consistent with the PJO–dTSI index relationship (Figure 10a), the regression of the NAO index against the dTSI index (Figure 10b) showed an area of positive NAO index around the zero phase angle contour. However, the simulated NAO index values and their statistical significance were much smaller than those obtained from the observation data, despite the much greater temporal extent of the dataset. Thus, we should rely more on the existence of coherent or meaningful structures in the regressed pattern rather than local strength of the statistical significance. It is noteworthy that the positive NAO signal appeared earlier in winter as the number of lag years increased, as was the case for both the recent and historical observational data sets. The positive NAO signal appeared one to two months earlier in the simulated data, although this may be a result of model bias. Note that this bias is common for many CMIP5 models (see Fig. 7 of Mitchell et al., 2015)

We next considered the effect of the solar cycle on the NAO in terms of the time evolution of key atmospheric quantities as a function of lag years and its evolution during the winter months (Figure 11). In association with the 11-year solar cycle, both the DJF-mean temperature at the equatorial stratopause and the November-mean subtropical meridional temperature gradient at the stratopause tended to peak at lags of 0 or –1 years. At the 0-year lag, the state vector in PJO space tended to intersect the positive PC1 axis from December to January, and the amplitude of the January-mean NAO index tended to peak, although the amplitude of the PJO index continued to increase until the 2-year lag (Figure 11a). The seasonal evolution of the PJO and the NAO indices for 0-lag years showed that the amplitudes of both tended to increase until they peaked in January (Figure 11b). Note also that the phase angle of the PJO intersected zero in January.

Note that the PJO indices, which are based on December or January (rather than January or February) means, are shown in Figure 11a because the timing of the downward movement of the modeled PJO tended to be earlier than that of the observational data. We consider this to reflect a model bias. In addition, the tendency of all of the regressed values to be very small reflects the much weaker correlation between these parameters and the dTSI index.

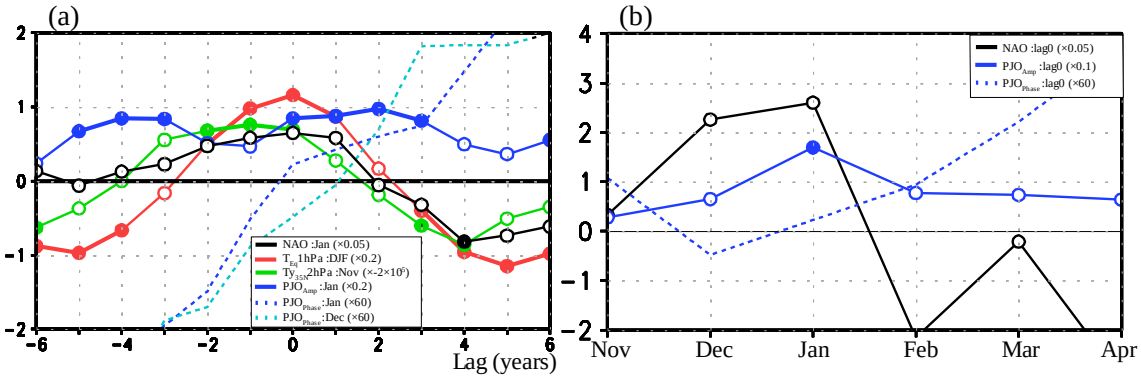

Figure 11. (a) Lagged regression of various simulated atmospheric quantities against annual mean dTSI index from 1850 to 2014. Positive lags correspond to years when solar activity leads the dTSI index. (b) Winter evolution of the NAO-index and PJO-indices regressed against annual mean dTSI index at 0-year lag. The values of atmospheric quantity at each point on its curve can be calculated by multiplying the corresponding value on the *y*-axis by the number in parentheses in the legend description. The units of measure for equatorial temperature at 1 hPa ($T_{eq}1hPa$), meridional gradient of temperature at 35°N and 2 hPa ($Ty_{35N}2hPa$), and phase of the PJO index (PJO_{phase}) are K, K m^{-1}, and degrees, respectively. On each curve, thick lines and closed circles indicate statistical significance higher than 80%.

To examine long-term changes in the solar–NAO relationship, 41-year running lagged regression of the December-January (DJ) mean NAO index is calculated in Figure 12a. Our examination (Figure 12a) showed that the peak of the NAO signal tended to drift slowly between lags of about –2 and +2 years (Figure 12a). It was at a lag of about –2 years for the period centered at 1890, shifted to a lag of about +2 years for the period centered at about 1930, and remained at +2 until about 1950, after which it drifted slowly to a lag of about 0 for the period centered at about 1970. The amplitude of the NAO was highest around 1890, but by about 1970 it was lower and remained low thereafter.

To examine the time of appearance of the NAO signal in winter and its longer term changes, we ran the above regressions without lag for two-winter-month periods (Figure 12c). This analysis showed that the NAO signal tended to appear in December–January throughout the period analyzed and to have its highest positive amplitudes for periods centered around 1900 and 1980.

Kuroda and Kodera (2004) have shown that NAO signals are strongly affected by the PJO. To examine long-term variations of the PJO, we therefore ran the same regression to the regression in Figure 12a, but for December–January mean PJO indices (Figure 12b). This analysis showed that the zero phase angle of the PJO tended to lie around 0-lag years, but with small shifts between lags of –2 and +2 years throughout the

period analyzed. The amplitude of the PJO was higher around lags of –1 and +4 years until around 1930, but decreased in amplitude during the period 1930–1950. After 1950, PJO amplitudes tended to be higher and moved gradually as the years passed to positive lag years.

We also examined the longer term changes of PJO indices by running the same regression as above but for the December–January mean variation of phase angle for 0-lag years (Figure 12e). This analysis showed that the phase angle stayed within ±50° throughout the period. Kuroda and Kodera (2004) have reported that the positive NAO tends to appear around the zero phase angle of the PJO, which is consistent with our result (Figure 12c). Note also that the NAO peaks around 1890 and lag of –2 years (Figure 12d). Thus, the positive NAO tended to be dominant in December–January throughout the entire 1850–2013 period.

Our results show that the appearance of the NAO tended to be closely related to the PJO and is thus an indication of stratosphere–troposphere coupling. The persistence of the near-zero phase angle for the December–January mean PJO around 0-lag years throughout 1850–2013 suggests strong monthly dependence of the solar cycle on the PJO, although the modeled progression of the PJO is somewhat faster than that indicated by the observed data (cf. Figures 5b and 11b). Thus, the long-term variation of the NAO appears to be influenced not by the PJO alone, but will be also strongly affected by ocean dynamics. The 50-year scale drift of the December–January mean NAO will be a consequence of oceanic influence.

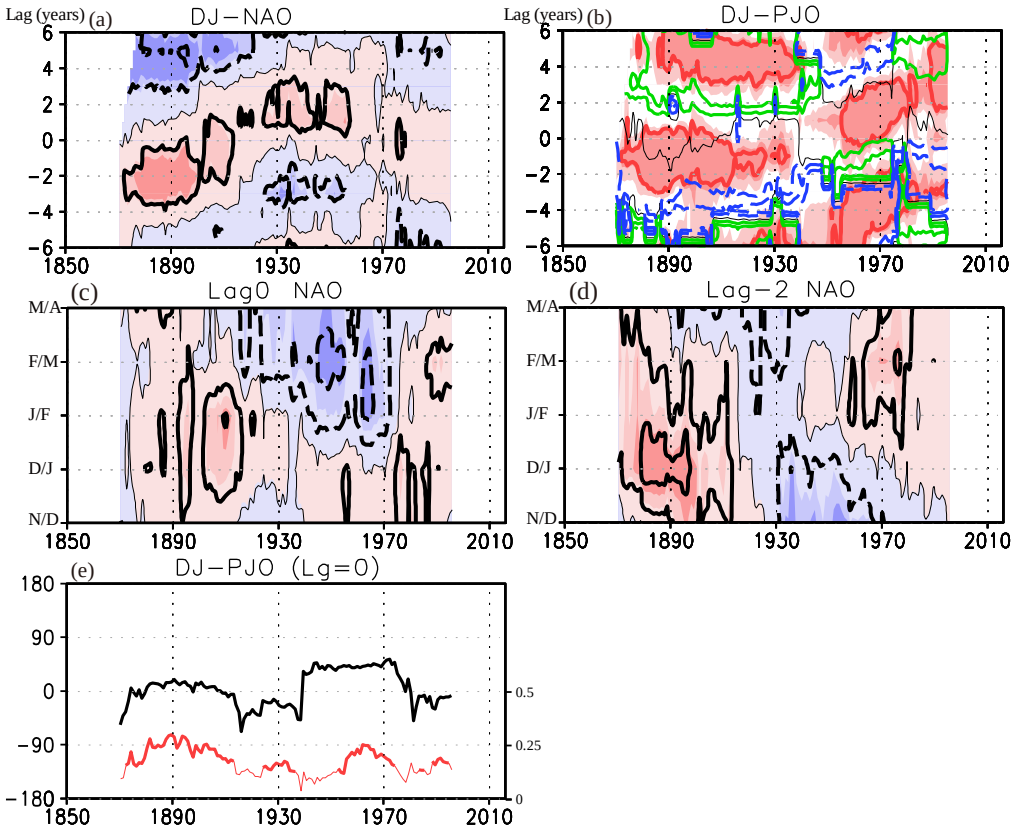

718

719

720 **Figure 12.** (a) 41-year running lagged regression of the simulated December–January (DJ)-mean NAO
721 index (contours) against annual mean dTSI data from 1850 to 2013. The *x*-axis shows the central years
722 for each of the 41-year running calculations at yearly increments. The shading indicates polarity (red
723 positive, blue negative). The darkest (middle) shading indicates greater than 90% (80%) statistical
724 significance. The contour interval is 0.2 and the thin line is the zero contour. (b) Same as (a) but for
725 DJ-mean PJO indices. The thick red contour is amplitude 0.2, and the shading indicates statistical
726 significance for the PJO amplitudes. The colored contours are phase angle (interval 60°). The thin
727 black line is the zero phase-angle contour and the solid green (dashed blue) line indicates positive
728 (negative) values. (c) Same as (a) but for the lag 0 regression of the NAO index for two-winter-month
729 periods. The contour interval is 0.15 and the thin line is the zero contour. (d) Same as (a) but for the
730 lag -2 regression of the NAO index for two-winter-month periods. (e) DJ-mean phase angle (black,
731 degrees) and amplitude (red, right-hand labels) of the PJO at 0-lag years. Positive lags indicate years
732 when solar activity leads. Thick red lines indicate statistical significance higher than 80 %.

733

734 Thus, we examined lagged regressions of solar-related SST and compared them
735 to those of the historical observation data. For this purpose, we defined the SST-NAO
736 index in the same way as in the historical observations, but excluding the area from
737 45°N to 60°N and 80°W to 45°E, where SST showed large variability. The lagged
738 regression of monthly SST-NAO index against the dTSI index (Figure 13a) shows the
739 SST-NAO peak signal at lags of about +3 and –6 years and that the seasonal variation of
740 the solar signal is small, although it tends to be stronger in early winter. It is noteworthy
741 that for positive lag years the overall pattern is very similar to that of the observation
742 data (Figure 8e). The 41-year running mean lagged regression of the SST-NAO index
743 for January using all monthly data (Figure 13b) produced very similar signals to those
744 of each winter month if the same calculations are performed by treating monthly mean
745 values as annual values. From about 1900 to 1960 (when the solar-related signal was
746 stronger), the SST-NAO tended to lag the DJ-NAO index (green lines in Figure 13b) by
747 1 to 3 years. In fact, the peak of the SST-NAO index was at lag 3 years, whereas the
748 peak for the DJ-NAO index was at lags of 1 to 2 years around 1940. Note that the larger
749 amplitude of the SST-NAO index around 1940 corresponds to largest lag of the DJ-
750 NAO index. The close relation of these signals suggests a close relation between solar-
751 forced NAO and SST. The resemblance of the solar-related SST-NAO signal to that of
752 the DJ-NAO index also supports this relationship.

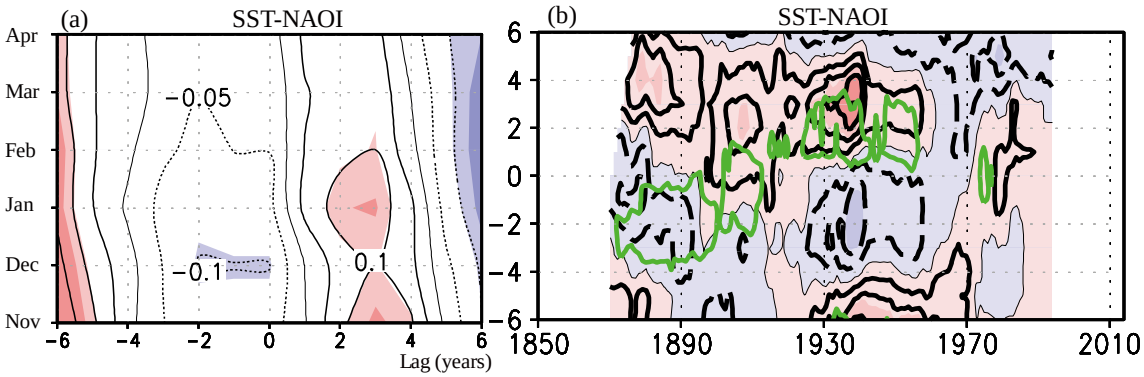

Figure 13. (a) Lagged regression of the simulated SST-NAO index (contours) against the dTSI index for 1850 to 2014. The contour interval is 0.05. The *x*-axis shows lag years; a positive lag means dTSI leads SST-NAO. Red and blue shading indicate positive and negative values, respectively. Areas of darker (lighter) shading indicate statistical significance higher than 90% (80%). (b) Lagged regression of the January SST-NAO index (contours) against monthly dTSI from 1850 to 2014. The *x*-axis shows the central years for each of the 41-year running mean calculations at yearly increments. The *y*-axis shows lag years. The contour interval is 0.1. Red and blue shading indicate positive and negative values, respectively. Areas of darker (lighter) shading indicate statistical significance higher than 90% (80%). The green contours show the same regression for the value of 0.2, but using the December-January-mean NAO index.

4. Discussion

We examined the influence of the 11-year solar cycle on the NAO by performing lagged regression analyses on both recent and historical observations, and on long-term historical simulation data obtained by using an Earth system model with projected external forcings. The analyses of observational data showed that a positive NAO signal develops at the surface in February at around the time of the solar maximum in response to activity of the PJO that is triggered by anomalous early winter westerly winds at the subtropical stratopause that are driven by solar radiation in the tropics. Because the phase of the PJO associated with the positive NAO tends to be reached earlier in winter as the lag in years increases, the NAO tends to become positive earlier in winter as the lag in years increases. The relationships of the historical observational data set and the long-term simulated historical dataset with the NAO were comparable. For the simulated historical data, the relationships among the subtropical stratopause temperature, the phases of the PJO and NAO, and the 11-year solar cycle were reasonable. The analyses of these two data sets also showed that the solar–NAO

relationship tended to drift around the mean state on a longer timescale; this drift suggests an oceanic influence on the NAO because the solar-related SST-NAO tends to have a close relation with the NAO of the key month: the SST-NAO tends to lag 2 to 3 years relative to the NAO when amplitudes of both indices are sufficiently large.

In recent years, the solar influence on the winter-mean NAO has been examined in both observational and modeling studies. For example, Gray et al. (2013, 2016) have examined historical SLP data and SSNs for the periods 1870–2010 and 1660–2010, respectively. They found the appearance of the positive peak of the NAO signal to be delayed by a few years relative to the peak solar year. Scaife et al. (2013) performed numerical experiments using the UK Met Office climate model and obtained a similar result, although they performed idealized transient simulations using an amplitude of UV variation that was likely too high. We repeated the same lagged regression analyses for the DJF-mean NAO using recent, historical observations and long-term simulated data, which showed that the peak of the NAO lagged by 0, +1 to +2, and –1 years, respectively (not shown).

Thus, the relationship between the solar cycle and winter-mean NAO that we determined disagree with results of Gray et al. (2013, 2016) and Scaife et al. (2013): we obtained a near-zero lag, whereas they obtained positive lags of 3–4 years. However, in our historical analysis of the 194-year (1823–2016) observational dataset, the DJF-mean NAO peak with a lag of +1 to +2 years may represent the influence of lagged response of the SST (Figure 8e). Also it should be noted that for shorter timescales the timing of the peak tended to drift. Similarly, the historical 165-year simulation (1850–2014) also showed an DJF-mean NAO peak at a lag of about –1 year, but the timing of the peak drifted when the dataset was subdivided into shorter periods. This drift would be related to the interaction of the ocean with the NAO. In particular, strength of this interaction with oceanic activity at the surface would have cause the NAO peak to drift from one period to another and prevented us from obtaining a valid estimate of the peak timing, even by using a very long-term dataset.

According to the results we obtained from observational data, however, solar-related variations of the NAO index occurred on a sub-seasonal timescale, corresponding with the speed of propagation of the PJO. Therefore, analyses of the NAO at a monthly time scale were necessary to capture the solar–NAO relationship. Without monthly data, an important characteristic of the solar–NAO relationship including the existence of the key month to the top-down mechanism, cannot be detected. Monthly data will also be needed to demonstrate the appearance of a positive

NAO signal earlier in winter with increasing years after peak solar activity. Sub-seasonal variations of the solar-related SST-NAO (Figures 8e, 13a) suggest that enhancement of the solar-related NAO at a few years lag of early winter is a direct result of the SST response, and the lagged response of SST is a result of the thermal inertia of the ocean. On the other hand, the enhanced solar-related SST signal in early winter (Figures 6, 10b) is a response to the tendency of the NAO to be more strongly affected by SST during early winter (Czaja and Frankignoul, 2002).

However, even if monthly data were available, 50-year-scale fluctuations of the timing of the peak NAO signals at key times (e.g., February of lag 0 years) would prevent statistically valid capture of the interaction of the solar–NAO signal with oceanic dynamics. Thus, the solar-related NAO signal cannot be captured by a simple spectral analysis method such as that of Chiodo et al. (2019). In fact, the solar-related NAO signal tends to be more prominent only during specific months (e.g., February), and even if a specific month is chosen for analysis, the NAO peak of that month may also drift at a 50-year scale. Therefore, the spectral structure of the solar-related NAO signal will be very complex. Development of a new method designed specifically to capture the solar-related signal from such complex data is needed.

To examine more directly the effect of the solar cycle on long-term ocean dynamics, we used the SST-NAO derived from monthly observation data (Figure 8e and 8f) to show that the SST-NAO signal was sometimes in phase with the solar cycle with a positive lag of 2 to 3 years, similar to the NAO signal in February. During these periods, both signals tended to be amplified, thus suggesting them to be strongly coupled. Although the periods when the SST-NAO was in phase with the solar cycle were not very long, the February NAO and the SST-NAO indices tended to be well correlated throughout the period 1854–2016. Thus, because the winter SST-NAO and February-NAO tended to be closely related when the SST-NAO signal was in phase with the solar cycle, we suggest that the February NAO signal tended to drive SST, and this forcing interacted with decadal oceanic dynamics to create an SST signal in phase with the solar cycle (Kodera et al., 2016) and amplified both the SST-NAO and NAO signals. The results of our simulations also support this mechanism.

To more directly assess the relationship between the solar cycle and the decadal component of the NAO, we compared the time series of the solar cycle and decadal components of the February-mean NAO index obtained from observed data (Figure 14a) or the December–January mean of the NAO index obtained from simulated data (Figure 14b). The decadal component of the NAO index was calculated by treating these monthly

mean values as annual values and filtering to extract frequencies from 8 to 15 years using the Lanczos band-pass filter with a window width of 31 years (Hamming, 1977). Comparison of the SSN with the decadal NAO from the observational data (Figure 14a) showed that the maxima and minima of the solar cycles were almost synchronous throughout the period analyzed, although there was some phase drift between cycles. The peaks matched reasonably well around years 1850, 1860, 1885, 1905, 1925, 1938, 1980, 1990, 2000, and 2010. The 41-year running correlations between SSN and decadal NAO were positive throughout the period analyzed. In contrast, the decadal component of the SST-NAO at a lag of 2 years correlated well with SSN only for limited periods of time (Figure 8f). This synchronicity of the decadal component of the NAO with the solar cycle likely represents a nonlinear response of the ocean, as pointed out by Thiéblemont et al. (2015).

Comparison of the TSI and decadal NAO from simulated data (Figure 14b) also showed good synchronicity throughout the period analyzed, with peaks matching reasonably well around years 1860, 1870, 1885, 1895, 1905, 1918, 1970, 1990, and 2000, although the match was poor around 1940. The 41-year running correlations between the TSI and decadal NAO were positive throughout. It should be noted that the solar synchronous component of the NAO was extracted from annual data, which means that the component was completely annually locked and reflected forcing of the PJO. Thus, both top-down and oceanic mechanisms appeared to be active in the solar–NAO system.

Thus, synchronicities of the solar cycle and the decadal component of the NAO occur only when signals of specific months are selected, which suggests that the monthly solar signal tends to be locked, but the signal is nearly synchronized with the NAO when considered decadally. This is an interesting phenomenon. Though Chiodo et al. (2019) claims the solar signal since the mid-1960s is a chance occurrence due to internal variability, it will not, if we look at Figure 14a.

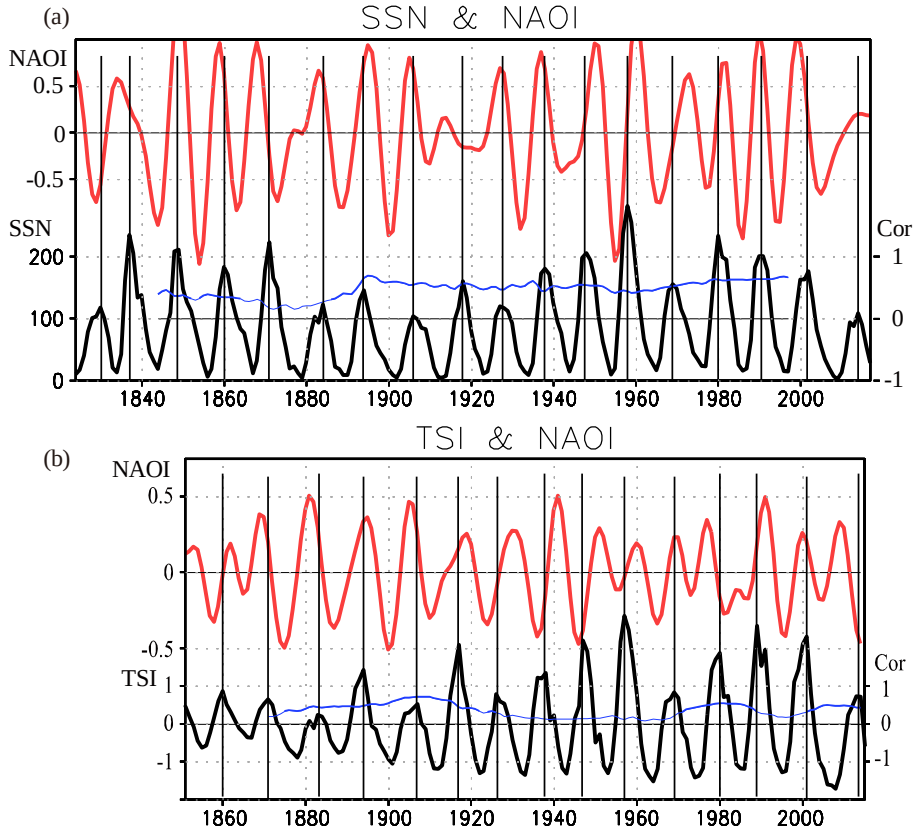

Figure 14. Comparison of observed and simulated NAO index and solar indices. (a) Decadal component of the February-mean NAO index (red line) and SSN from observation data. Peaks of SSN are marked by vertical black lines. Forty-one-year running correlations between NAO index and SSN are shown by the blue line with the right label. Correlation greater than 95% significance level is shown by thick line. (b) Same as (a) but for simulated DJ mean NAO index (red line) and TSI. Running correlations of TSI are again shown by blue line. On both panels, vertical lines mark solar maxima.

Neither the solar signal of the NAO (Figure 12a) nor the synchronicity of the decadal NAO and the solar cycle (Figure 14b) are as strongly evident in our simulation results as they are in the observational data. Moreover, the period covered by our simulation is relatively short, so it may be better to regard our simulation results as some reference in the present. Although our simulation results had some features in common with the observed solar–NAO relationship, it may be possible to derive more congruence by running historical simulations over longer time intervals. Future analyses incorporating more historical simulations (e.g., CMIP6 simulations) or performing ensemble runs will be useful in this regard.

5. Conclusions

The results of our analysis suggest that the solar–NAO relationship is created by a top-down mechanism modulated by the ocean. A possible effect of the ocean is evident in our monthly mapping of the time of appearance in winter of the NAO, which showed that the NAO tended to appear earlier in winter as the lag in years increased. If formation of the NAO were entirely a top-down mechanism, there would be no asymmetry between positive- and negative-lag years. The agent of this asymmetry will be the thermal inertia of the ocean. Another indication of an oceanic effect is the drift we identified of the timing of the peak NAO relative to solar maximum years on a 50-year timescale. This drift suggested the existence of a strong nonlinear interaction between the solar cycle and ocean dynamics. The modulation of the decadal component of the NAO also suggested such an interaction. The direct relationship between the solar cycle and ocean dynamics requires further examination.

Acknowledgments

This research was supported in part by Grants-in-Aid for Scientific Research (26287115, 26281016, 16H01184, 18H01280) from the Ministry of Education, Culture, Sports, Science and Technology of Japan. The ERA-Interim data is available from the ECMWF website (https://www.ecmwf.int/en/forecasts/datasets/reanalysis-datasets/era-interim). Monthly data of the F10.7 index are available from the Natural Resources Canada website (https://www.spaceweather.gc.ca/solarflux/sx-5-en.php). The sources of satellite data sets are https://rda.ucar.edu/datasets/ds067.1/, https://rda.ucar.edu/datasets/ds067.3, and https://rda.ucar.edu/datasets/ds067.4/ for the NCEP/CPC, and https://aura.gsfc.nasa.gov/science/data.html for the Aura-MLS. Historical NAO index was obtained from the University of East Anglia Climate Research Unit, UK website (https://crudata.uea.ac.uk/~timo/datapages/naoi.htm). Historical sun spot numbers were obtained from the Royal Observatory of Belgium website (http://www.sidc.be/silso/datafiles). Historical SST data was obtained from the NOAA website (https://www.ncdc.noaa.gov/data-access/marineocean-data/extended-reconstructed-sea-surface-temperature-ersst-v5). The numerical data used in this study are available from https://climate.mri-jma.go.jp/pub/archives/Kuroda-et-al_Solar_NAO_MRI-ESM2.0.

Appendix A

Following Kuroda and Kodera (2004), we defined the Polar-night Jet

Oscillation (PJO) and its index by the two leading empirical orthogonal functions (EOFs) and their principal component (PC) time series of anomalous polar temperatures from 1000 to 1 hPa levels during extended winter (November to April) by using ERA-Interim data (Figure A1, top panels). Almost 90% of the variance in polar temperatures was explained by these two EOFs. For calculation of EOFs, the physical thickness (meters) of each pressure level was considered, and polar temperature was defined as the monthly average temperature poleward of 80°N. Because the amplitude of the PJO signal in the troposphere is negligible, the PJO is a result of mostly stratospheric variability.

We also calculated the regression of zonal-mean zonal wind against each PC time series (Figure A1, lower panels). The state vector tended to rotate counterclockwise with time when represented in two-dimensional space (PJO-space) represented by the principal component 1 (PC1) (*x*-axis) and PC2 (*y*-axis). This counterclockwise rotation of the state vector corresponds to the poleward and downward shift of the anomalous zonal-mean zonal wind with time, which Kuroda and Kodera (2001) have defined as the temporal evolution of the PJO. Correlation of PC1 (PC2) with the NAO index is 0.28 (–0.15) if all 6×38 months are used, and both indices are then related to the NAO index at greater than 99% statistical significance.

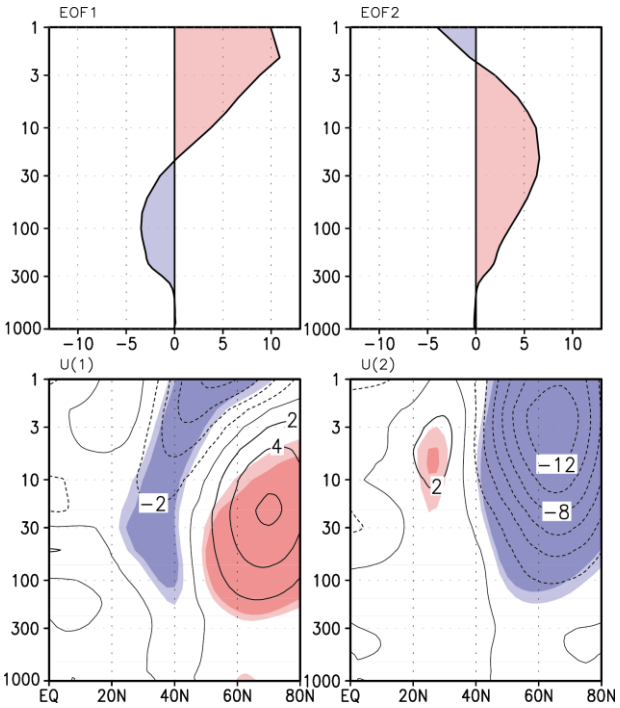

Figure A1. Upper panels: Vertical profiles of the EOF1 (left) and EOF2 (right) of anomalous northern winter polar cap temperatures. Lower panels: Regressions of time series of zonal-mean zonal winds against the EOF1 (left) and EOF2 (right). The *y*-axes are height (hPa). The *x*-axes of

upper panels are temperature (K), those of lower panels are latitude. Dark (light) shading (red positive, blue negative) indicates areas of greater than 99% (95%) statistical significance.

References

Andrews, D. G., J. R. Holton, and C. B. Leovy (1987), *Middle Atmosphere Dynamics* (489 pp.), Orlando: Academic Press.

Andrews, M. B., Knight, J. R., & Gray L. J. (2015). A simulated lagged response of the North Atlantic Oscillation to the solar cycle over the period 1960-2009. *Environmental Research Letters, 10,* 1–10. https://doi.org/10.1088/1748-9326/10/5/054022

Bailey, S. M, C. A. Barth, and S. C. Solomon (2002), A model of nitric oxide in the lower thermosphere, *Journal of Geophysical Research: Atmospheres, 107*(A8), 1205, https://doi.org/10.1029/2001JA000258.

Chiodo, G. et al. (2016), The impact of a future solar minimum on climate change projection in the northern hemisphere. *Environmental Research Letters, 11,* 034015. https://doi.org/10.1088/1748-9326/11/3/034015.

Chiodo, G., Oehrlein, J., Polvani, L. M., Fyfe, J. C., & Smith A. K. (2019), Insignificant influence of the 11-year solar cycle on the North Atlantic Oscillation. *Nature Geoscience 12*, 94–99. https://doi.org/10.1038/s41561-018-2293-3

Czaja, A. and C. Frankignoul (2002), Observed impact of Atlantic SST anomalies on the North Atlantic Oscillation, *J. Clim., 15,* 606-623, https://doi.org/10.1175/1520-0442(2002)015<0606:OIOASA>2.0.C;2.

Dee, D. P. et al. (2011), The ERA-Interim reanalysis: configuration and performance of the data assimilation system, *Quarterly Journal of the Royal Meteorological Society, 137,* 553–597, https://doi.org/doi:10.1002/qj.828.

1025 Dhomse, S.S., et al. (2016), On the ambiguous nature of the 11 year solar cycle signal in
1026 upper stratosphere ozone. *Geophysical Research Letters, 43*, 7241-7249, https://
1027 doi.org/doi:10.1002/2016GL069958.
1028 Eyring, V. et al. (2016), Overview of the Coupled Model Intercomparison Project Phase
1029 6 (CMIP6) experimental design and organization, *Geoscientific Model Development*,
1030 9, 1939-1958, https://doi.org/doi:10.5194/gmd-9-1937-2016.
1031 Gray, L. J. et al. (2010), Solar influence on climate, *Revew of Geophysics, 48,* RG4001,
1032 https://doi.org/doi:10.1029/2009RG000282.
1033 Gray, L. J. et al., (2013), A lagged response to the 11 year solar cycle in observed winter
1034 Atlantic/European weather patterns, *Journal of Geophysical Research: Atmospheres,*
1035 *108,* 13,405-13,420, https://doi.org/doi:10.1029/2013JD020062.
1036 Gray, L. J., T. J. Woollings, M. Andrews, and J. Knight, (2016), Eleven-year solar cycle
1037 signal in the NAO and Atlantic / European blocking, *Quarterly Journal of the Royal*
1038 *Meteorological Society, 142,* 1890-1903, https://doi.org/doi:10.1002/1j.2782.
1039 Hamming, R. W. (1977), *Digital Filters*, pp. 296, Prentice Hall, Englewood Cliffs, N.J.
1040 Hines, C. O., (1997), Doppler-spread parameterization of gravity-wave momentum
1041 deposition in the middle atmosphere. 2. Broad and quasi-monochromatic spectra, and
1042 implementation, *Journal of Atmospheric and Solar-Terrestrial Physics, 59*, 387-400.
1043 Huang, B., et al., (2017), Extended Reconstructed Sea Surface Temperature, Version 5
1044 (ERSSTv5): Upgrades, Validations, and Intercomparisons.
1045 Hurrell, J. W., Y. Kushnir, G. Ottersen, and M. Visbeck, (edit) (2003), *The North Atlantic*
1046 *Oscillation*, Geophysical Monographs, vol. 134, pp. 279, American Geophysical
1047 Union, Washington, DC.
1048 Ineson, S., A. A. Scaife, J. R. Knight, J. C. Manners, N. J. Dunstone, L. J. Gray, and J. D.

1049 Haigh (2011), Solar forcing of winter climate variability in the northern hemisphere,
1050 *Nature Geoscience*, 4, 753-757, https://doi.org/doi:10.1038/NGEO1282.
1051 Jones, P.D., T. Jonsson, and D. Wheeler (1997), Extension to the North Atlantic
1052 Oscillation using early instrumental pressure observations from Gibraltar and South-
1053 West Iceland, *Int. J. Climatol.* 17, 1433-1450. https://doi.org/doi:10.1002/(SICI)1097-
1054 0088(19971115)17:13<1433::AID-JOC203>3.0.CO;2-P.
1055 Kodera, K. (1995), On the origin and nature of the interannual variability of the winter
1056 stratospheric circulation in the northern hemisphere, *Journal of Geophysical Research:*
1057 *Atmospheres, 1070*(D7)*,*14,077-14,087, https://doi.org/doi:10.1029/95JD01172.
1058 Kodera, K., and Y. Kuroda, (2002), Dynamical response to the solar cycle, *Journal of*
1059 *Geophysical Research: Atmospheres, 107*(D24)*,*4749,
1060 https://doi.org/doi:10.1029/2002JD002224.
1061 Kodera, K., R. Thiéblemont, S. Yukimoto, and K. Matthes (2016), How can we
1062 understand the global distribution of the solar cycle signal on the Earth's surface?
1063 *Atmos. Chem. Phys., 16,* 12925-12944, https://doi.org/10.5194/acp-16-12925-2016.
1064 Kopp, G. and J. L. Lean (2011), A new, lower value of total solar irradiance: Evidence
1065 and climate significance, *Geophysical Research Letters, 38*, L01706,
1066 https://doi.org/doi:10.1029/2010GL045777.
1067 Kuroda, Y., and K. Kodera (2001), Variability of Polar-night jet in the northern and
1068 southern hemispheres, *Journal of Geophysical Research: Atmospheres, 106 (D18)*, 20,
1069 703-20, 713, https:doi.org/10.1029/2001JD900226.
1070 Kuroda, Y., and K. Kodera (2002), Effect of solar activity on the polar-night jet oscillation
1071 in the northern and southern hemisphere winter, *Journal of the Meteorological Society*
1072 *of Japan, 80,* 973-984, https://doi.org/10.2151/jmsj.80.973.

1073 Kuroda, Y., and K. Kodera (2004), Role of the polar-night jet oscillation on the formation
1074 of the Arctic Oscillation in the northern hemisphere winter, *Journal of Geophysical*
1075 *Research: Atmospheres,109,* D11112, https://doi.org/doi:10.1029/2003JD004123.
1076 Lean, L. et al., (1997), Detection and parameterization of variations in solar mid and near-
1077 ultraviolet radiation (200-400 nm). *Journal of Geophysical Research: Atmospheres,*
1078 *102 (D25)*, 29, 939-29, 956, https://doi.org/10.1029/97JD02092.
1079 Ma, H., H. Chen, L. Gray, L. Zhou, X. Li, R. Wang, and S. Zhu, (2018), Changing
1080 response of the North Atlantic/European winter climate to the 11 year solar cycle,
1081 *Environmental Research Letters, 13*, 034007, https://doi.org/10.1088/1748-
1082 9326/aa9e94.
1083 Maisel, L. (1971), *Probability, statistics and random processes*, (280pp.) New York,
1084 Simon & Schuster, Inc.
1085 Matthes, K., U. Langematz, L. Gray, K. Kodera, and Labitzke, K. (2004), Improve 11-
1086 year solar signal in the Freie Universitaet Berlin Climate middle atmosphere Model
1087 (FUB-CMAM), *Journal of Geophysical Research: Atmospheres,* D06101,
1088 https://doi.org/doi:10.1029/2003JD004012.
1089 Matthes, K., Y. Kuroda, K. Kodera, and U. Langematz, (2006), Transfer of the solar signal
1090 from the stratosphere to the troposphere: Northern winter, *Journal of Geophysical*
1091 *Research: Atmospheres, 111,* D06108, https://doi.org/doi:10.1029/2005JD006283.
1092 Matthes, K. et al. (2017), Solar forcing for CMIP6 (v3.2), *Geoscientific Model*
1093 *Development Discussions, Copernicus Publications, 10 (6)*, 2247-2302,
1094 https://doi.org/doi:10.5194/gmd-10-2247-2017.
1095 Meehl, G. A., J. M. Arblaster, K. Matthes, F. Sassi, H. van Loon (2009), Amplifying the
1096 Pacific climate system response to a small 11-year solar cycle forcing, *Science, 325*,

1114-1118, https://doi.org/doi:10.1126/science.1172872.

Misios S. et al. (2019), Slowdown of the walker circulation at solar cycle maximum, PNAS, 116, 7186-7191, https://doi:10.1073/pnas.1815060116.

Mitchell D. M. et al. (2015), Solar signals in CMIP-5 simulations: the stratospheric pathway, *Q. J. R. Meteorol. Soc., 141*, 2390-2403, https://doi.org/doi:10.1002/qj.2530.

Scaife, A. A., S. Ineson, J. R. Knight, L. Gray, K. Kodera, and D. M. Smith, A mechanism for lagged North Atlantic climate response to solar variability (2013), *Geophysical Research Letters, 40*, 434-439, https://doi.org/doi:10.1002/grl.50099.

Schwartz, M. J. et al. (2008), Validation of the Aura microwave limb sounder temperature and geopotential height measurements, *Journal of Geophysical Research: Atmospheres, 103,* D15S11, https://doi.org/doi:10.1029/2007JD008783.

Spiegl, T., and U. Langematz (2020), Twenty-first-century climate hot spots in the light of a weakening sun, *Journal of Climate 33*, 3431-3447, https://doi.org/10.1175/JCLI-D-19-0059.1

Thiéblemont, R., K. Matthes, N-E. Omirani, K. Kodera, and F. Hansen (2015), Solar forcing synchronized decadal North Atlantic climate variability, *Nature Communications, 6:8268,* https://doi.org/doi:10.1038/ncomms9268.

Yukimoto, S., et al. (2012), A new Global Climate Model of the Meteorological Research Institute: MRI-CGCM3 -Model description and basic performance, *Journal of the Meteorological Society of Japan,* 90A, 23-64, http://doi.org/10.2151/jmsj.2012-A02.

Yukimoto, S., et al. (2019), The MRI Earth System Model version 2.0, MRI-ESM2.0: Description and basic evaluation of the physical component, *Journal of the Meteorological Society of Japan,* 97, 931-965, http://doi.org/10.2151/jmsj.2019-051.